

# Self-Elongation with Sequential Folding of a Filament of Bacterial Cells

Ryojiro Honda <sup>\*</sup>, Jun-ichi Wakita <sup>†</sup> and Makoto Katori <sup>‡</sup>

*Department of Physics, Faculty of Science and Engineering,  
Chuo University, Bunkyo, Tokyo 112-8551, Japan*

21 September 2015

## Abstract

Under hard-agar and nutrient-rich conditions, a cell of *Bacillus subtilis* grows as a single filament owing to the failure of cell separation after each growth and division cycle. The self-elongating filament of cells shows sequential folding processes, and multifold structures extend over an agar plate. We report that the growth process from the exponential phase to the stationary phase is well described by the time evolution of fractal dimensions of the filament configuration. We propose a method of characterizing filament configurations using a set of lengths of multifold parts of a filament. Systems of differential equations are introduced to describe the folding processes that create multifold structures in the early stage of the growth process. We show that the fitting of experimental data to the solutions of equations is excellent, and the parameters involved in our model systems are determined.

## 1 Introduction

Patterns observed in bacterial colonies growing on surfaces of semisolid agar plates realize a variety of fractal and self-affine structures studied in statistical mechanics and fractal physics [1]. In a series of experimental studies [2, 3, 4, 5], it has been clarified that the morphology of growing bacterial colonies at the macroscopic scale does not depend on the biological details of individual organisms, but depends only on environmental conditions controlled by the agar concentration  $C_a$  and the nutrient concentration  $C_n$ . Cell motility is changed by varying  $C_a$  and the growth rate is controlled by varying  $C_n$ , and then different

---

<sup>\*</sup>E-mail:rhonda@phys.chuo-u.ac.jp

<sup>†</sup>E-mail:wakita@phys.chuo-u.ac.jp

<sup>‡</sup>E-mail:katori@phys.chuo-u.ac.jp

patterns appear in different regions in a morphology diagram drawn on the  $C_a$ - $C_n$  plane. On this plane, a diffusion-limited aggregation (DLA)-like pattern [6, 7], an Eden-like pattern [8, 9], a concentric-ring pattern, a homogeneously spreading disk like pattern, and a dense branching morphology (DBM) pattern [1] have been recorded. Since some of these patterns are observed not only in biological systems, but also in chemical and physical systems, such as those in crystal growth, aggregation processes, and viscous fingering [10], the mechanism of pattern formation could be common in organisms and inorganic substances, and a theoretical study by mathematical modeling and analysis will be useful for understanding the underlying universal principles [11, 12, 13, 14, 15].

In a recent paper [16], we have reported the physical aspects of the collective motion of bacterial cells observed in shallow circular pools prepared on the surface of an agar plate. The diameters of the pools are arranged so as not to be much larger than the length of the bacterial cells swimming in the pools. We used *Bacillus (B.) subtilis* and found six different types of collective motion, including one-way and two-way rotational motion along the brim of a circular pool and collective oscillatory motion in the entire pool. Analyzing experimental observations in 117 circular pools, we found that these six types of collective motion can be classified using only two parameters: the reduced cell length  $\lambda$ , which is defined as the ratio of the average cell length in a pool to the pool diameter, and the cell density  $\rho$  in the pool. We obtained a phase diagram for the collective motion drawn on the  $\lambda$ - $\rho$  plane and predicted that simple modeling with the two control parameters will be able to explain the variety of collective motion of bacterial cells.

The above results imply that physical considerations are applicable and useful to explain the changes in the morphology of bacterial colonies at the macroscopic scale as well as the dynamical transitions of the collective motion of bacterial cells at the microscopic scale caused by environmental variations. On the basis of them, in this paper, we will report the experimental results and numerical analyses of growth processes starting from a single bacterial cell observed in formation of colony patterns. We tried to analyze the observed growth process by fractal analysis and by using systems of differential equations.

Throughout the experiment reported in this paper, we used *B. subtilis* wild-type strain OG-01. Cells of this strain are rod-shaped (0.5–1.0  $\mu\text{m}$  in diameter, 2–5  $\mu\text{m}$  in length) with peritrichous flagella. They swim in a straight line in water by bundling and rotating the flagella. Under unfavorable environmental conditions, such as on a nutrient-poor medium or a dry agar plate, they become spores. When a small number of cells are inoculated on the surface of a semisolid agar plate, they go through a resting period of about 7 h before starting two-dimensional colony expansion.

As briefly reported in previous papers [3, 17], we observed string like objects in microscopy observations of an inoculation spot of a bacterial suspension in the later stage of the resting phase. In this study, we focus on the growth process that started from a single bacterial cell in the resting period under hard-agar and nutrient-rich conditions. In this case, cell multiplications are repeated with a constant cell cycle (doubling time), but daughter cells fail to separate after each cell cycle, although the cytoplasm has been compartmentalized by septum formation. Then, a long filament is produced, which consists of a chain of cells linked end to end [18]. Such a filament writhes as it elongates on the agar plate, and eventually



Figure 1: Snapshot of the filament configuration of bacterial cells on an agar plate at time  $t = 40$  min after the first twofold part appeared. The scale bar indicates  $20 \mu\text{m}$ .

some segment starts folding and a twofold part of the filament is created. Figure 1 shows a typical configuration of a filament in which twofold parts have been created. Sooner or later, we will see the appearance of threefold parts, fourfold parts, and so forth, and the filament configuration of linked cells becomes complicated on the agar plate.

Mendelson and coworkers have intensively studied the supercoiling processes performed by such cell filaments of *B. subtilis* [18, 19, 20, 21, 22]. They are interested in the situation wherein the filaments twist to make a double-stranded helix. The double-stranded structure itself twists while writhing, eventually comes in contact with itself, and forms a supercoil. By the repetition of such supercoiling processes, macroscopic structures of millimeter length are created, which are called bacterial macrofibers. The interesting motion of macrofibers was reported by Mendelson and coworkers. [23, 24, 25, 26]. Kumada *et al.* also observed the growth of filaments of cells without separation for *B. subtilis*, in which the dependence of the morphology on  $C_a$  was systematically studied [27]. Such growing filamentous cells were also observed for *Escherichia (E.) coli* [28].

In this paper, we study the simplest situation wherein a filament of bacterial cells does not twist, and hence helical structures are not formulated. In our case, a single self-elongating filament repeatedly folds upon itself and shows a crossover from a one-dimensional structure to a two-dimensional structure. In Sect. 2, we explain the experimental setup and procedure for recording microscopic snapshots of cell filament configurations for about 6 h. We performed fractal analysis of filament configurations by the box-counting method. In Sect. 3, we report that the results imply fractal structures in the filament configurations, and the evaluated fractal dimension  $D$  shows a crossover from  $D = 1$  to 2 as the growth process goes from the exponential phase to the stationary phase. Detailed study of the time evolution of the filament configuration of bacterial cells is discussed in Sects. 4 and 5. In Sect. 4, we propose a method of characterizing filament configurations on an agar plate by a set

of lengths of the simple part and the  $k$ -fold parts with  $k = 2, 3, 4, \dots$ , and the results of experimental measurements of these lengths are shown. To analyze the data given in Sect. 4, we introduce systems of differential equations in Sect. 5 and the nonlinear fitting of data to their solutions is performed. Section 6 is devoted to concluding remarks.

## 2 Experimental Procedures

We observe a multiple-fission process from a single bacterial cell in the resting period under hard-agar and nutrient-rich conditions. The experimental setup and procedure are as follows.

A solution containing 5 g of sodium chloride (NaCl), 5 g of dipotassium hydrogen-phosphate ( $K_2HPO_4$ ) and 10 g of Bacto-Peptone (Becton, Dickinson and Company, Franklin Lakes, NJ, USA) in 1 L of distilled water is prepared. The environmental parameter  $C_n$  is given as the concentration of Bacto-Peptone;  $C_n = 10 \text{ g}\cdot\text{L}^{-1}$ . Then, the solution is adjusted to pH 7.1 by adding 6 N hydrochloric acid (HCl). Moreover, the solution is mixed with 10 g of Bacto-Agar (Becton, Dickinson and Company), which determines the softness of a semisolid agar plate. The environmental parameter  $C_a$  is given as the concentration of Bacto-Agar;  $C_a = 10 \text{ g}\cdot\text{L}^{-1}$ . The environmental condition realized by these values of  $C_a$  and  $C_n$  gives a typical Eden-like pattern of *B. subtilis* colonies. The mixture is autoclaved at 121 °C for 15 min, and 20 mL of the solution is poured into each sterilized plastic petri dish of 88 mm inner diameter. The thickness of the semisolid agar plates is about 3.2 mm. After solidification at room temperature for 60 min, the semisolid agar plates are dried at 50 °C for 90 min.

3  $\mu\text{L}$  of the bacterial suspension is inoculated at the center of each agar plate surface. 1  $\mu\text{L}$  of the suspension includes about  $10^2$  cells in the spore state. The agar plates are left at room temperature for about 60 min to dry the bacterial suspension droplet. Thereafter, they are cultivated in a stage top incubator at 35 °C (INULG2-OTOR-CV, Tokai Hit, Shizuoka), which is attached to the stage of an optical microscope (IX71, Olympus, Tokyo). The spores at the inoculated center spot germinate about 2 h after the inoculation. They repeatedly undergo cell multiplications without splitting or movement, and form a long filament. The filament of cells linked in tandem grows two-dimensionally on the agar plate surface like a self-elongating string. This growth process of a filament of cells is observed through an optical microscope with a 20x objective.

A digital camera (DP71, Olympus, Tokyo) is connected to the optical microscope. Microscopy snapshots are recorded every minute for about 6 h using bio-imaging analysis software (Lumina Vision, Mitani, Fukui and Tokyo) from the time when spore germination occurred to the time when the entanglement of a filament started two-dimensional colony expansion.

### 3 Crossover from One-Dimensional Structure to Two-Dimensional Structure

In this section, the time after the inoculated spot germinated is denoted by  $T$  [min]. Let  $L(T)$  [ $\mu\text{m}$ ] be the total length of a filament of bacterial cells observed at time  $T$ . If the specific growth rate is denoted by  $\mu$ , it will show an exponential elongation,

$$L(T) = L(0)e^{\mu T}, \quad T \geq 0. \quad (3.1)$$

First, we confirmed that the observed  $L(T)$  data up to  $T = 200$  min are well described by the single exponential function Eq. (3.1), and the specific growth rate was evaluated to be

$$\mu = 3.58 \times 10^{-2} \text{ min}^{-1}. \quad (3.2)$$

This gives a cycle time (doubling time) of

$$\tau = \frac{\ln 2}{\mu} = 19.4 \text{ min}. \quad (3.3)$$

The snapshots of filament configurations at  $T = 125$  and  $245$  min are shown on the left-hand side in Fig. 2 with a resolution of  $2040 \times 1536$  pixels. They are analyzed by the box-counting method to evaluate the fractal dimensions of the filament configurations of bacterial cells on the agar plate. The procedure is as follows. At each time  $T$ , the snapshot picture is divided by squares (two-dimensional boxes) of linear size  $\varepsilon$ , and then is counted the number  $N_T(\varepsilon)$  of squares containing the pixels occupied by the filament of bacterial cell. If the configuration has a fractal structure,  $N_T(\varepsilon)$  is scaled as

$$N_T(\varepsilon) \sim \varepsilon^{-D(T)} \quad (3.4)$$

with the fractal dimension  $D(T)$ . We changed the value of  $\varepsilon$  from 1 to 1536 pixels (from  $2.1 \times 10^{-1}$  to  $3.2 \times 10^2 \mu\text{m}$  in the real scale). As shown in the log-log plots given on the right-hand side in Fig. 2, the data for  $T = 125$  min show a power law in the range of  $3.5 \mu\text{m} < \varepsilon < 5.6 \times 10^1 \mu\text{m}$  in the real scale, and those for  $T = 245$  min show a power law in the range of  $2.5 \mu\text{m} < \varepsilon < 2.1 \times 10^1 \mu\text{m}$  in the real scale. The slopes  $-1.16$  and  $-1.96$  in these log-log plots in Fig. 2 provide the fractal dimensions  $D(125) = 1.16$  and  $D(245) = 1.96$ , respectively. The result implies that the filament configurations have fractal structures. We evaluated the fractal dimensions of the filament at  $T = 45, 85, 165, 205, 285, 325$ , and  $365$  min and the results are plotted in Fig. 3. We found that the data can be fitted to the following sigmoid function:

$$D(T) = c_1 \tanh[\sigma(T - T_0)] + c_2 \quad (3.5)$$

with  $T_0 = 1.82 \times 10^2$  min,  $\sigma = 1.61 \times 10^{-2} \text{ min}^{-1}$ ,  $c_1 = 5.1 \times 10^{-1}$ , and  $c_2 = 1.54$ . The time evolution of the multiple fission of bacterial cells from the exponential phase to the stationary phase is well described by the time dependence of the fractal dimension of the filament configuration on the agar plate.

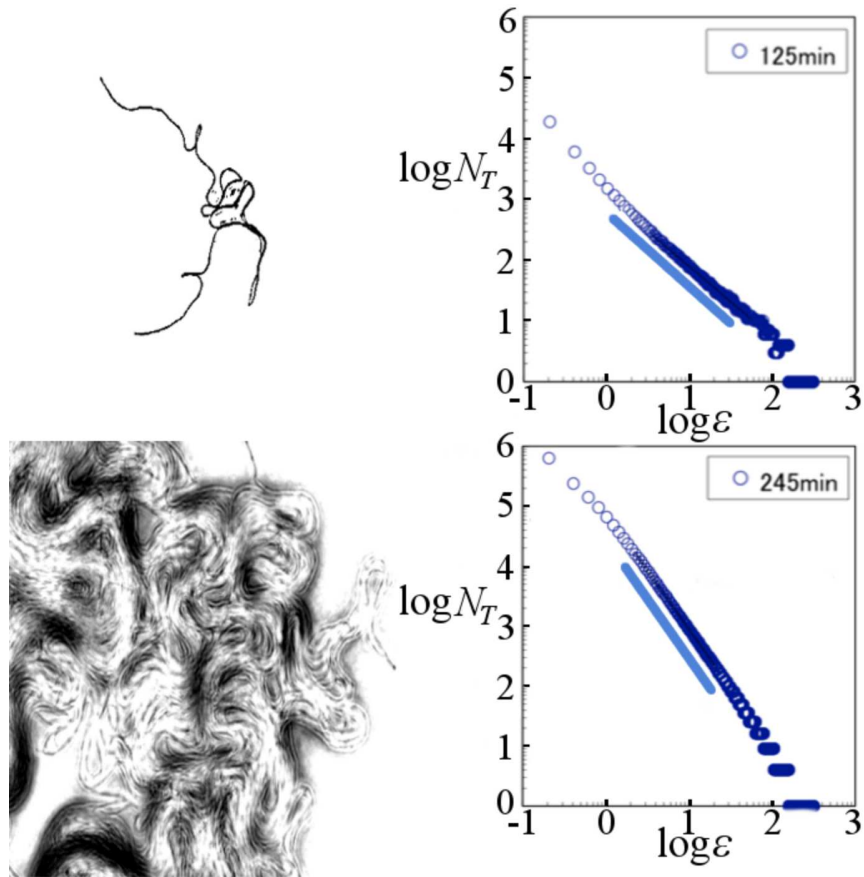


Figure 2: (Color online) Upper left (lower left) picture: snapshot of the cell filament at time  $T = 125$  min ( $T = 245$  min). The upper right (lower right) graph shows the log-log plots of  $N_T(\varepsilon)$  versus  $\varepsilon$ . We find linear regions in the log-log plots, and the fractal dimensions of the filament configurations are evaluated as  $D(125) = 1.16$  and  $D(245) = 1.96$ , respectively.

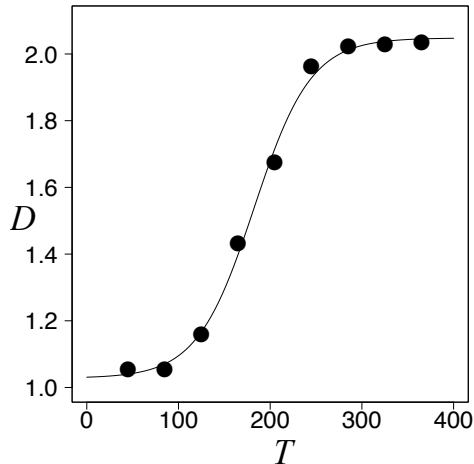


Figure 3: Time dependence of fractal dimension  $D(T)$  of the filamentous cell configuration on the agar plate. The data are well described by the sigmoid function given by Eq. (3.5).

## 4 Folding Processes and Experimental Measurements

In this section, we denote the observation time by  $t$  [min] instead of  $T$  [min], since we will set  $t = 0$  at the time when the first folding of a filament occurs as explained below.

Let  $L(t)$  [ $\mu\text{m}$ ] be the total length of a filament of bacterial cells at time  $t$ . Here, we write the specific growth rate as  $\alpha$ , and then  $L(t)$  should obey the following differential equation:

$$\frac{d}{dt}L(t) = \alpha L(t). \quad (4.1)$$

On the semisolid agar plate, the linear growth is unstable, and a filament of cells starts folding after a short time. It repeats the folding processes and the configuration of the filament on the plate becomes complicated very rapidly. Over time, the multifold structure becomes dense and its region spreads over the plates. In this way, the configuration of a filament of cells shows a crossover from the one-dimensional structure to the two-dimensional structure, as shown in the previous section.

In an interval of a filament, if bacterial cells are linked in tandem and form a curved line without folding, the interval is called a simple segment. At each time  $t$ , we consider the union of all simple segments in a filament and call it the simple part. We represent its length by  $l_1(t)$  [ $\mu\text{m}$ ]. As illustrated by [1] in Fig. 4, we see the following process:

Elementary Process [1] : elongation of a simple segment,

and  $l_1(t)$  rapidly increases with time  $t$ .

We set  $t = 0$  at the time when the first folding of a filament is observed. In this experiment,  $t = T - 60$  [min]. For  $t > 0$ , the following process occurs:

Elementary Process [2] : creation of a twofold segment by folding of a simple segment,

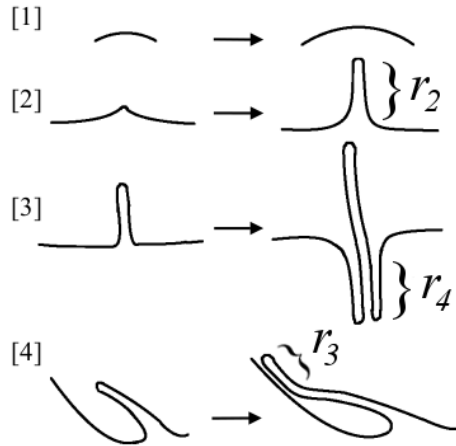


Figure 4: Illustrations of elementary processes found in the self-elongating process of a filament of bacterial cells in the early stage. [1] Elongation of simple segment. [2] Creation of a twofold segment by folding a simple segment. Twice the length  $r_2$  is added to the length  $l_2$ . [3] Creation of a fourfold segment by elongation of a twofold segment. Four times the length  $r_4$  is added to the length  $l_4$ . [4] Creation of a threefold segment by folding of a twofold segment on a simple segment. Three times the length  $r_3$  is added to the length  $l_3$ .

as illustrated by [2] in Fig. 4. The twofold part is defined by the union of all twofold segments in the filament, whose length is denoted by  $l_2(t)$  [ $\mu\text{m}$ ]. By definition,  $l_1(t) = L(t), l_2(t) = 0$  for  $t \leq 0$ , while  $l_1(t) = L(t) - l_2(t), l_2(t) > 0$  for  $t > 0$ . Sooner or later, we will see threefold segments, fourfold segments, and so forth. We call the union of all  $k$ -fold segments the  $k$ -fold part, and write the length of the  $k$ -fold part as  $l_k(t)$  [ $\mu\text{m}$ ],  $k = 2, 3, 4, \dots$ . See the elementary processes [3] and [4] in Fig. 4, which create a fourfold segment and a threefold segment, respectively. We will attempt to characterize the time evolution of the filament configuration of cells using the set of lengths  $(l_1(t), l_2(t), l_3(t), \dots)$  developing in time  $t$ . Since  $\sum_{k \geq 1} l_k(t) = L(t)$ , the data are regarded as a time-dependent ‘partition’ of an exponentially growing length  $L(t)$ .

We found a critical time  $t_*$  such that when  $0 \leq t \leq t_*$ , the whole filament of cells consists of only simple segments and twofold segments, while when  $t > t_*$ , we observe the appearance of threefold and fourfold segments in a filament of cells and the configuration starts to become complicated. In this experiment, we observed

$$t_* = 45 \text{ min.} \quad (4.2)$$

It corresponds to the time  $T_* = t_* + 60 = 105$  min after the inoculated spot germinated. Note that it gives the time when the fractal dimensions  $D(T)$  of the filament starts to show its rapid increase in Fig. 3.

Figure 5 shows a snapshot of a configuration of bacterial cells at  $t = 60$  min. We obtained an enlarged photocopy of the snapshot picture and traced the filament segments by hand.



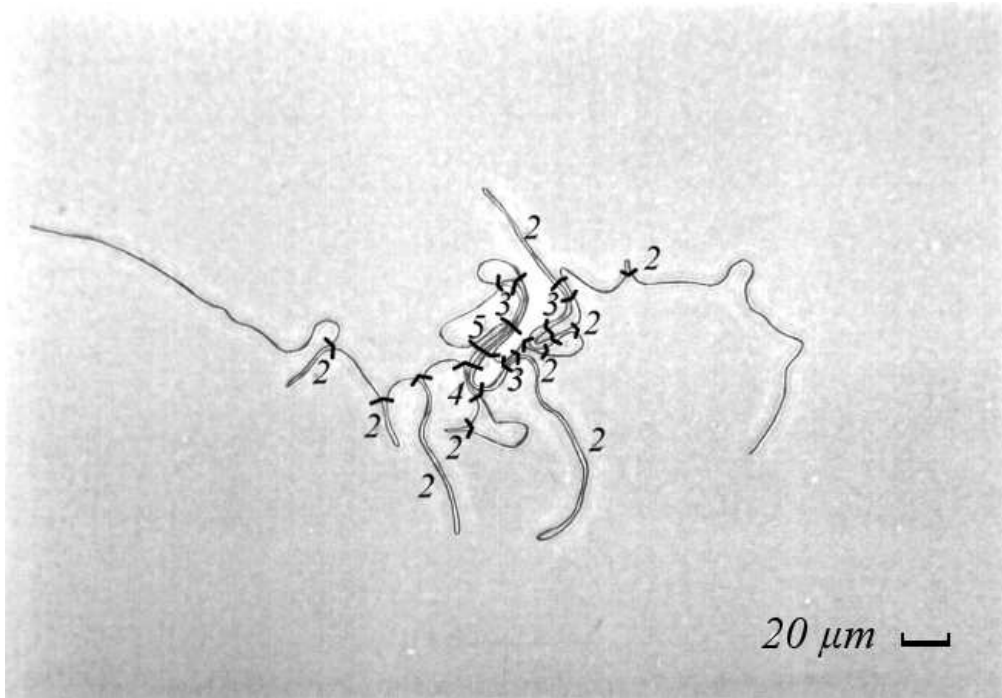


Figure 5: Snapshot of a configuration of the filament of bacterial cells at time  $t = 60$  min. Each interval with a number  $k$  represents a  $k$ -fold segment of the filament, where  $k = 2, 3, 4,$  and  $5$ . The intervals without a number are the simple segments. The scale bar indicates  $20 \mu\text{m}$ .

Each interval with a number  $k$  represents a  $k$ -fold segment of the filament, where  $k = 2, 3, 4,$  and  $5$ . The intervals without a number are the simple segments. We used an opisometer, which is an instrument for measuring the length of arbitrary curved lines on a sheet. If the length of a segment indexed  $k$  is  $r_k$ , the length  $l_k(t)$  of the  $k$ -fold part of the filament should be the sum of  $kr_k$  over all  $k$ -fold segments. We measured  $(l_k(t))_{k \geq 1}$  up to time  $t = 90$  min. The results are listed in Table 1, where the lengths of parts with  $k \geq 3$  are summed and the values of  $l_{3+}(t) = \sum_{k \geq 3} l_k(t)$  are given. In the experiment, we fixed the field of vision of the optical microscope. Just before  $t = 70$  min, a tip of the simple part ran out of the field of vision, and after  $t = 70$  min, twofold segments may have been created out of our field of vision. Hence, the values of  $L$  and  $l_1$  at  $t = 70, 80,$  and  $90$  and those of  $l_2$  at  $t = 80$  and  $90$  are not given in Table 1.

## 5 Analysis by Systems of Differential Equations

### 5.1 Exponential growth of total length

Equation (4.1) is solved as

$$L(t) = Ae^{\alpha t}. \quad (5.1)$$

Table 1: Experimental data.

$t$ [min]	$L$ [ $\mu\text{m}$ ]	$l_1$ [ $\mu\text{m}$ ]	$l_2$ [ $\mu\text{m}$ ]	$l_{3+}$ [ $\mu\text{m}$ ]
0	151	151	0	0
10	228	189	39	0
20	315	247	68	0
30	485	340	145	0
40	733	442	291	0
50	1070	620	362	90
60	1590	810	584	197
70	—	—	944	535
80	—	—	—	1260
90	—	—	—	2710

Here,  $A = L(0)$  is the total length of the filament at  $t = 0$  when the first folding occurs.

As shown in Fig. 6, the time dependence of  $L(t)$  is described by Eq. (5.1) very well for  $0 \leq t \leq 60$  min, and we obtained the following values by the semilog fitting of the data:

$$\alpha = 3.95 \times 10^{-2} \text{ min}^{-1}, \quad A = 1.50 \times 10^2 \mu\text{m}. \quad (5.2)$$

The evaluation of  $\alpha$  is consistent with the evaluation given by Eq. (3.2) for the specific growth rate  $\mu$  averaged over the longer time period  $0 \leq T \leq 200$  min.

## 5.2 Systems of differential equations and their solutions

In the time interval  $0 \leq t \leq t_*$ , only elementary processes [1] and [2] take place. We assume that in the elongation process of a cell filament with specific growth rate  $\alpha$ , the ratio of the frequency of elementary process [2] to that of elementary process [1] is given by  $\beta/(1 - \beta)$  with a constant  $0 < \beta < 1$ . Then, the time evolution of the lengths  $l_1(t)$  and  $l_2(t)$  will be described by the following system of linear differential equations:

$$\begin{aligned} \frac{d}{dt}l_1(t) &= \alpha(1 - \beta)l_1(t), \\ \frac{d}{dt}l_2(t) &= \alpha l_2(t) + \alpha\beta l_1(t), \quad 0 \leq t \leq t_*. \end{aligned} \quad (5.3)$$

Note that the first term in the second equation in Eq. (5.3) describes the self-elongation process of the twofold part. Since we have set  $t = 0$  at the time when the first folding occurs, Eq. (5.3) should be solved under the conditions

$$l_1(0) = L(0) = A, \quad l_2(0) = 0. \quad (5.4)$$

The solution is then given by

$$\begin{aligned} l_1(t) &= Ae^{\alpha(1-\beta)t}, \\ l_2(t) &= Ae^{\alpha t}(1 - e^{-\alpha\beta t}), \quad 0 \leq t \leq t_*. \end{aligned} \quad (5.5)$$

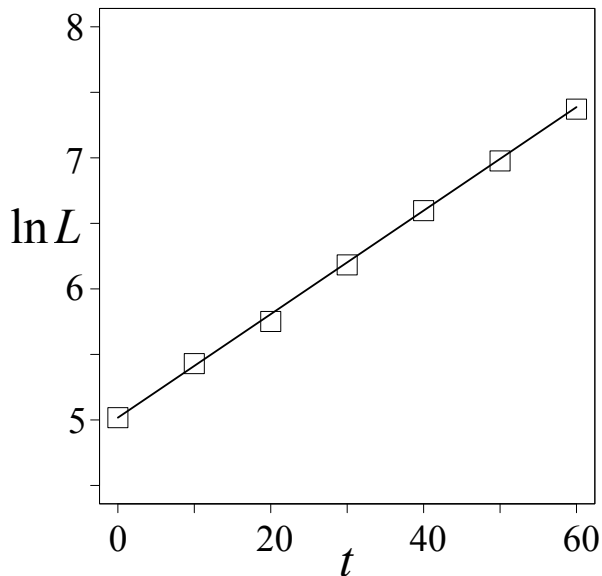


Figure 6: Values of  $\ln L(t)$  plotted for  $t = 0, 10, 20, \dots, 60$  min. The linear fitting of Eq. (5.1) in this semilog plot determines the values of  $\alpha = 3.95 \times 10^{-2} \text{ min}^{-1}$  and  $A = 1.50 \times 10^2 \mu\text{m}$ .

For  $t > t_*$ , we take into account the following elementary processes in addition to processes [1] and [2]:

Elementary Process [3] : creation of a fourfold segment by elongation of a twofold segment,

Elementary Process [4] : creation of a threefold segment by folding of a twofold segment on a simple segment.

As illustrated by [3] in Fig. 4, a part of the elongating twofold segments becomes a fourfold segment. We assume that the ratio of the frequency of fourfold segment creation to that of simple elongation of the twofold part is given by  $\gamma/(1 - \gamma)$  with a constant  $0 < \gamma < 1$ . As illustrated by [4] in Fig. 4, the creation of threefold segments can occur only if a twofold segment touches a simple segment and folds on it and if they merge into a threefold segment. Thus, its frequency will be proportional to the product of  $l_1(t)$  and  $l_2(t)$ . We assume that this process reduces the total length of the simple part by  $\delta_1 l_1(t) l_2(t)$  and that of the twofold part by  $\delta_2 l_1(t) l_2(t)$  with transition rates per unit length  $\delta_1 > 0$  and  $\delta_2 > 0$ . Then, if we set  $l_{3+}(t) = \sum_{k \geq 3} l_k(t) = l_3(t) + l_4(t) + \dots$ , we will obtain the following system of nonlinear

differential equations:

$$\begin{aligned}
\frac{d}{dt}l_1(t) &= \alpha(1-\beta)l_1(t) - \delta_1 l_1(t)l_2(t), \\
\frac{d}{dt}l_2(t) &= \alpha(1-\gamma)l_2(t) + \alpha\beta l_1(t) - \delta_2 l_1(t)l_2(t), \\
\frac{d}{dt}l_{3_+}(t) &= \alpha l_{3_+}(t) + \alpha\gamma l_2(t) + (\delta_1 + \delta_2)l_1(t)l_2(t), \quad t \geq t_*.
\end{aligned} \tag{5.6}$$

We assume that the parameters  $\delta_1$  and  $\delta_2$  are sufficiently small and solve the system of nonlinear differential equations given by Eq. (5.6) by perturbation. This assumption will be verified by the data fitting as explained in Sect. 5.3.

For  $k = 1, 2$ , and  $3_+$ , we expand  $l_k(t)$  as power series of  $\delta_1$  and  $\delta_2$  as

$$\begin{aligned}
l_k(t) &= \sum_{m_1=0}^{\infty} \sum_{m_2=0}^{\infty} \delta_1^{m_1} \delta_2^{m_2} \tilde{l}_k^{(m_1, m_2)}(t) \\
&= \sum_{n=0}^{\infty} \sum_{\substack{m_1 \geq 0, m_2 \geq 0, \\ m_1 + m_2 = n}} \delta_1^{m_1} \delta_2^{m_2} \tilde{l}_k^{(m_1, m_2)}(t),
\end{aligned} \tag{5.7}$$

where  $\tilde{l}_k^{(m_1, m_2)}(t)$  are time-dependent coefficients of the expansion. The  $N$ th-order approximate solution,  $N = 0, 1, 2, \dots$ , is given by

$$l_k^{(N)}(t) = \sum_{n=0}^N \sum_{\substack{m_1 \geq 0, m_2 \geq 0, \\ m_1 + m_2 = n}} \delta_1^{m_1} \delta_2^{m_2} \tilde{l}_k^{(m_1, m_2)}(t), \quad k = 1, 2, 3_+. \tag{5.8}$$

In the following, we calculate the 0th- and first-order approximate solutions:

$$\begin{aligned}
l_k^{(0)}(t) &= \tilde{l}_k^{(0,0)}(t), \\
l_k^{(1)}(t) &= l_k^{(0)}(t) + \delta_1 \tilde{l}_k^{(1,0)}(t) + \delta_2 \tilde{l}_k^{(0,1)}(t), \quad k = 1, 2, 3_+, \quad t \geq t_*.
\end{aligned} \tag{5.9}$$

The 0th-order approximate solution,  $\{l_k^{(0)}(t) : k = 1, 2, 3_+\}$ , solves the system of linear differential equations obtained from Eq. (5.6) by setting  $\delta_1 = \delta_2 = 0$ . In addition to the initial conditions corresponding to Eq. (5.4),

$$l_1^{(0)}(0) = A, \quad l_2^{(0)}(0) = 0, \tag{5.10}$$

the definition of the critical time  $t_*$  gives

$$l_{3_+}^{(0)}(t_*) = 0. \tag{5.11}$$

Under these conditions, we have the following:

$$\begin{aligned}
l_1^{(0)}(t) &= Ae^{\alpha(1-\beta)t}, \\
l_2^{(0)}(t) &= \frac{\beta A}{\beta - \gamma} e^{\alpha(1-\gamma)t} (1 - e^{-\alpha(\beta-\gamma)t}), \\
l_{3_+}^{(0)}(t) &= \frac{A}{\beta - \gamma} e^{\alpha t} \left\{ -\beta(e^{-\alpha\gamma t} - e^{-\alpha\gamma t_*}) + \gamma(e^{-\alpha\beta t} - e^{-\alpha\beta t_*}) \right\}, \quad t \geq t_*.
\end{aligned} \tag{5.12}$$

To express the first-order approximate solution, we introduce the multiple integrals

$$\begin{aligned}
I^{(1)}(t; t_*, a_1) &= \int_{t_*}^t ds e^{-a_1 s} l_1^{(0)}(s) l_2^{(0)}(s), \\
I^{(2)}(t; t_*, a_2, a_1) &= \int_{t_*}^t ds e^{-a_2 s} I^{(1)}(s; t_*, a_1), \\
I^{(3)}(t; t_*, a_3, a_2, a_1) &= \int_{t_*}^t ds e^{-a_3 s} I^{(2)}(s; t_*, a_2, a_1),
\end{aligned} \tag{5.13}$$

where  $a_i$ ,  $i = 1, 2$ , and  $3$  are constants. By inserting  $l_1^{(0)}(t)$  and  $l_2^{(0)}(t)$  given in Eq. (5.12), they are calculated as

$$\begin{aligned}
I^{(1)}(t; t_*, a_1) &= \frac{\beta A^2}{\beta - \gamma} \left\{ \frac{e^{(p-a_1)t} - e^{(p-a_1)t_*}}{p - a_1} - \frac{e^{(q-a_1)t} - e^{(q-a_1)t_*}}{q - a_1} \right\}, \\
I^{(2)}(t; t_*, a_2, a_1) &= \frac{\beta A^2}{\beta - \gamma} \left\{ \frac{e^{(p-a_1-a_2)t} - e^{(p-a_1-a_2)t_*}}{(p-a_1)(p-a_1-a_2)} - \frac{e^{(q-a_1-a_2)t} - e^{(q-a_1-a_2)t_*}}{(q-a_1)(q-a_1-a_2)} \right. \\
&\quad \left. + \frac{e^{-a_2 t} - e^{-a_2 t_*}}{a_2} \left( \frac{e^{(p-a_1)t_*}}{p-a_1} - \frac{e^{(q-a_1)t_*}}{q-a_1} \right) \right\}, \\
I^{(3)}(t; t_*, a_3, a_2, a_1) &= \frac{\beta A^2}{\beta - \gamma} \left[ \left\{ \frac{e^{(p-a_1-a_2-a_3)t} - e^{(p-a_1-a_2-a_3)t_*}}{(p-a_1)(p-a_1-a_2)(p-a_1-a_2-a_3)} \right. \right. \\
&\quad \left. \left. - \frac{e^{(q-a_1-a_2-a_3)t} - e^{(q-a_1-a_2-a_3)t_*}}{(q-a_1)(q-a_1-a_2)(q-a_1-a_2-a_3)} \right. \right. \\
&\quad \left. \left. - \frac{e^{-(a_2+a_3)t} - e^{-(a_2+a_3)t_*}}{a_2(a_2+a_3)} \left( \frac{e^{(p-a_1)t_*}}{p-a_1} - \frac{e^{(q-a_1)t_*}}{q-a_1} \right) \right\} \right. \\
&\quad \left. + \frac{e^{-a_3 t} - e^{-a_3 t_*}}{a_3} \left\{ \frac{e^{(p-a_1-a_2)t_*}}{(p-a_1)(p-a_1-a_2)} - \frac{e^{(q-a_1-a_2)t_*}}{(q-a_1)(q-a_1-a_2)} \right. \right. \\
&\quad \left. \left. + \frac{e^{-a_2 t_*}}{a_2} \left( \frac{e^{(p-a_1)t_*}}{p-a_1} - \frac{e^{(q-a_1)t_*}}{q-a_1} \right) \right\} \right],
\end{aligned} \tag{5.14}$$

where  $p = \alpha(2 - \beta - \gamma)$ ,  $q = 2\alpha(1 - \beta)$ .

Then, the first-order approximate solution is given by

$$\begin{aligned}
l_1^{(1)}(t) &= l_1^{(0)}(t) - \delta_1 e^{\alpha(1-\beta)t} I^{(1)}(t; t_*, \alpha(1 - \beta)), \\
l_2^{(1)}(t) &= l_2^{(0)}(t) - \delta_1 \alpha \beta e^{\alpha(1-\gamma)t} I^{(2)}(t; t_*, -\alpha(\gamma - \beta), \alpha(1 - \beta)) \\
&\quad - \delta_2 e^{\alpha(1-\gamma)t} I^{(1)}(t; t_*, \alpha(1 - \gamma)), \\
l_{3+}^{(1)}(t) &= l_{3+}^{(0)}(t) \\
&\quad + \delta_1 \left\{ -\alpha^2 \beta \gamma e^{\alpha t} I^{(3)}(t; t_*, \alpha \gamma, -\alpha(\gamma - \beta), \alpha(1 - \beta)) + e^{\alpha t} I^{(1)}(t; t_*, \alpha) \right\} \\
&\quad + \delta_2 \left\{ -\alpha \gamma e^{\alpha t} I^{(2)}(t; t_*, \alpha, \alpha(1 - \gamma)) + e^{\alpha t} I^{(1)}(t; t_*, \alpha) \right\}, \quad t \geq t_*.
\end{aligned} \tag{5.15}$$

Note that, owing to the initial condition  $l_1^{(1)}(0) = l_1^{(0)}(0) = A$ ,  $l_1^{(1)}(t)$  given in the first line of Eq. (5.15) becomes independent of  $\delta_2$ .

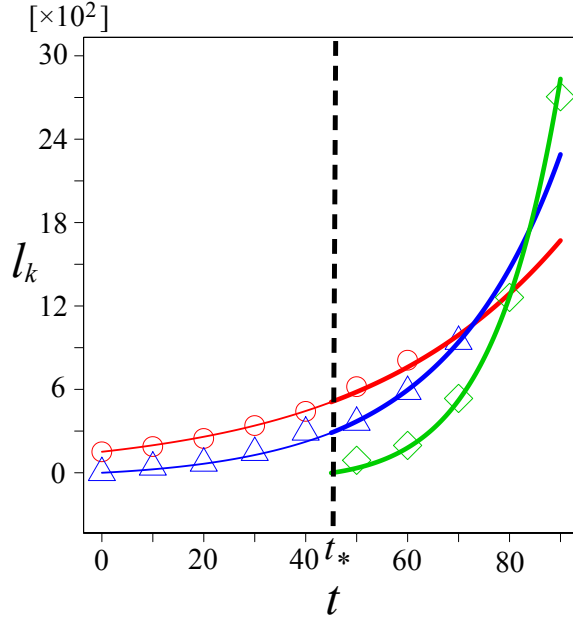


Figure 7: (Color online) Data of  $l_1(t)$ ,  $l_2(t)$ , and  $l_{3+}(t)$  plotted by  $\circ$ ,  $\triangle$ , and  $\diamond$ , respectively. The thin curves represent the solution given by Eq. (5.5) for  $0 \leq t \leq t_*$  with the parameters given by Eqs. (5.2) and (5.16). The solution given by Eq. (5.15) for  $t \geq t_*$  is represented by the thick curves, where the parameters are given by Eq. (5.17). The fitting is excellent.

### 5.3 Nonlinear fitting

First, we used five pairs of data  $(l_1(t), l_2(t))$  of  $t = 0, 10, \dots, 40 < t_* = 45$  in Table 1. Note that the parameters  $\alpha$  and  $A$  have already been determined using Eq. (5.2). By fitting to the solution given by Eq. (5.5) of the system given by Eq. (5.3) of linear differential equations for  $(l_1(t), l_2(t))$ ,  $0 \leq t \leq t_*$ , we obtained the value of parameter

$$\beta = 0.317. \quad (5.16)$$

Next, we used the data  $l_k(t)$ ,  $k = 1, 2$ , and  $3_+$  for  $t = 50, 60, \dots, 90 > t_* = 45$  in Table 1 and performed their nonlinear fitting to the first-order approximate solution given by Eq. (5.15) of the system of nonlinear differential equations given by Eq. (5.6). Here,  $A$ ,  $\alpha$ , and  $\beta$  are fixed to be the values given by Eqs. (5.2) and (5.16), and  $\gamma$ ,  $\delta_1$ , and  $\delta_2$  are chosen as fitting parameters. They are evaluated as

$$\begin{aligned} \gamma &= 0.313, \\ \delta_1 &= 6.24 \times 10^{-7} \text{ min}^{-1} \cdot \mu\text{m}^{-1}, \quad \delta_2 = 3.75 \times 10^{-8} \text{ min}^{-1} \cdot \mu\text{m}^{-1}. \end{aligned} \quad (5.17)$$

The fitting is excellent as shown by Fig. 7. The evaluation given by Eq. (5.17) is consistent with the assumption  $|\delta_i| \ll 1$ ,  $i = 1, 2$ , on which we solved the system of nonlinear differential equations given by Eq. (5.6) by perturbation in Sect. 5.2.

The nonlinearity is very small but necessary in the fitting. To demonstrate it, we show the 0th-order approximate solution given by Eq. (5.12) as curves in Fig. 8. Here, we used

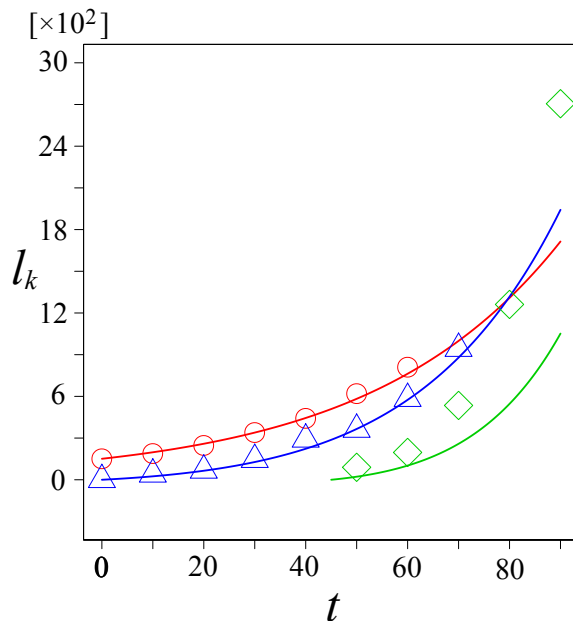


Figure 8: (Color online) Data of  $l_1(t)$ ,  $l_2(t)$ , and  $l_{3+}(t)$  plotted by  $\circ$ ,  $\triangle$ , and  $\diamond$ , respectively. The curves show the 0th-order solution given by Eq. (5.12), which ignores the nonlinear terms in Eq. (5.6). We failed to fit  $l_{3+}(t)$ .

the same values of  $A$ ,  $\alpha$ , and  $\beta$  as in Fig. 7, but we put  $\delta_1 = \delta_2 = 0$ . Figure 8 shows that if we ignore the nonlinear terms in Eq. (5.6), we fail to fit the data of  $l_{3+}(t)$ ,  $t \geq t_*$ .

## 6 Concluding Remarks

In this paper, we have reported that the growth process of cells of *B. subtilis* under hard-agar and nutrient-rich conditions allows the realization of the dynamics of a self-elongating filament with sequential folding on a plane. Such a multiple-fission process without cell separation is commonly observed in the early stage of the growth process even if the agar concentration is changed, while the structure and motion of an entangled filament of cells in the later stage depend on environmental conditions [18, 21, 3, 17, 27]. Takeuchi *et al.* reported a study on filamentous cells of *E. coli* [28]. Environmental conditions to realize such self-elongation of cell filaments should be clarified by a systematic study of the early stage of bacterial growth processes. The classification of the morphology and dynamics of a long filament of cells depending on environmental conditions, time periods, spatial and geometrical restrictions, and so forth will be an interesting future problem.

Here, we have focused on the simplest situation wherein a filament of cells simply repeats folding processes as it elongates and isotropically spreads over a two-dimensional plate. Note that Mendelson and coworkers have very extensively studied filamentous cell growth in the situation wherein supercoiling processes create helical macrofibers and their chiral self-propulsion motion is observed [18, 19, 20, 21, 22, 23, 24, 25, 26]. Even in our simple case, it

seems to be highly nontrivial to provide a proper description of the filament configuration, which rapidly becomes complicated as it elongates with sequential folding embedded in a plane. In this work, we have proposed describing the global development by the time-dependent fractal dimension  $D(T)$  and the local folding processes by the time evolution of partitions  $(l_k(t))_{k \geq 1}$  of the exponentially growing total length  $L(t)$  of the filament of cells, where  $k = 1$  for the simple part and  $k \geq 2$  for the  $k$ -fold parts.

The analysis discussed in Sect. 5 could be regarded as a mean-field-type approximation in the following sense. Let us consider a magnetic spin system on a lattice. In the mean-field theory, to describe a phase transition, we consider only the magnetization as an order parameter, which is obtained by averaging over spin configurations. The magnetization per spin  $m(T, H)$  at temperature  $T$  in an external magnetic field  $H$  is calculated by approximating the correlated many-spin system by a single-spin system in a mean field generated by the surrounding spins, which is assumed to be proportional to  $m(T, H)$ . The proportionality coefficient can be called the effective coupling constant  $J_{\text{eff}}$ . In this way, we obtain the self-consistency equation for  $m(T, H)$  with the parameter  $J_{\text{eff}}$  in addition to the external parameters  $T$  and  $H$ . If we want to compare the experimental data of a magnetization process of some material with the mean-field theory, the parameter  $J_{\text{eff}}$  should be evaluated by some additional experimental observation. In this analysis of the filament configuration with folding, we summed  $l_k(t)$  over  $k \geq 3$  to define  $l_{3+}(t)$ . By this reduction of variables from the series  $(l_k(t))_{k \geq 1}$  to the triplet  $(l_1(t), l_2(t), l_{3+}(t))$ , we obtained the finite systems of coupled differential equations given by Eq. (5.3) for  $0 \leq t \leq t_*$  and by Eq. (5.6) for  $t \geq t_*$ . They involve the parameters  $\alpha, \beta, \gamma, \delta_1$ , and  $\delta_2$ . We have evaluated these parameters as well as  $t_*$  by experimental observations.

As shown by Eqs. (5.16) and (5.17), the evaluated  $\beta$  and  $\gamma$  have almost the same value. We can verify that the quantities given by Eqs. (5.12) and (5.14) have finite values in the limit  $\gamma \rightarrow \beta$ , and then our first-order approximate solution given by Eq. (5.15) is also valid in the case where  $\beta = \gamma$ . We should note that if  $\beta = 1/3$  ( $\gamma = 1/3$ ), the ratio of the frequency of twofold-segment (fourfold-segment) creation to that of simple elongation of the single (twofold) part is given by  $\beta/(1 - \beta) = 1/2$  ( $\gamma/(1 - \gamma) = 1/2$ ). We will continue our study to answer the question whether this result,  $\beta \simeq \gamma \simeq 1/3$ , is universal.

To improve the description, we need to carry out further studies on growing elastic filaments. Theoretical investigations can be found in the literature [29, 30, 31, 32]. We hope that this experimental evaluations of parameters controlling the folding processes, which are described as  $l_1 \rightarrow l_2$ ,  $l_2 \rightarrow l_4$ , and  $l_1 + l_2 \rightarrow l_3$  using our variables, will be useful for testing the validity of a possible theoretical consideration in the future.

**Acknowledgments** JW was supported by a Chuo University Grant for Special Research and by a Grant-in-Aid for Exploratory Research (No. 15K13537) from Japan Society for the Promotion of Science. MK was supported in part by a Grant-in-Aid for Scientific Research (C) (No. 26400405) from Japan Society for the Promotion of Science.



## References

- [1] M. Matsushita, F. Hiramatsu, N. Kobayashi, T. Ozawa, Y. Yamazaki, and T. Matsuyama, *Biofilms* **1**, 305 (2004).
- [2] O. Rauprich, M. Matsushita, C. J. Weijer, F. Siegert, S. E. Esipov, and J. A. Shapiro, *J. Bacteriol.* **178**, 6525 (1996).
- [3] J. Wakita, H. Itoh, T. Matsuyama, and M. Matsushita, *J. Phys. Soc. Jpn.* **66**, 67 (1997).
- [4] H. Ito, J. Wakita, T. Matsuyama, and M. Matsushita, *J. Phys. Soc. Jpn.* **68**, 1436 (1999).
- [5] F. Hiramatsu, J. Wakita, N. Kobayashi, Y. Yamazaki, M. Matsushita, and T. Matsuyama, *Microbes Environ.* **20**, 120 (2005).
- [6] T. A. Witten and L. M. Sander, *Phys. Rev. Lett.* **47**, 1400 (1981).
- [7] P. Meakin, *J. Theor. Biol.* **118**, 101 (1986).
- [8] M. Eden, *in Proc. 4th Berkeley Symp. Mathematical Statistics and Probability*. ed. H. P. Newman (University of California Press, Berkeley, 1961) Vol. IV, p. 223.
- [9] F. Family and T. Vicsek, *J. Phys. A* **18**, L75 (1985).
- [10] T. Vicsek, *Fractal Growth Phenomena* (World Scientific, Singapore, 1992) 2nd ed.
- [11] T. Vicsek, A. Czirók, E. Ben-Jacob, I. Cohen, and O. Shochet, *Phys. Rev. Lett.* **75**, 1226 (1995).
- [12] T. Vicsek and A. Zafeiris, *Phys. Rep.* **517**, 71 (2012).
- [13] H. R. Brand, H. Pleiner, and D. Svensěk, *Eur. Phys. J. E* **34**, 128 (2011).
- [14] H. Pleiner, D. Svensěk, and H. R. Brand, *Eur. Phys. J. E* **36**, 135 (2013).
- [15] H. R. Brand, H. Pleiner, and D. Svensěk, *Eur. Phys. J. E* **37**, 83 (2014).
- [16] J. Wakita, S. Tsukamoto, K. Yamamoto, M. Katori, and Y. Yamada, to be published in *J. Phys. Soc. Jpn.*
- [17] J. Wakita, H. Kuninaka, T. Matsuyama, and M. Matsushita, *J. Phys. Soc. Jpn.* **79**, 094002 (2010).
- [18] N. H. Mendelson, *Proc. Natl. Acad. Sci.* **73**, 1740 (1976).
- [19] N. H. Mendelson: *Proc. Natl. Acad. Sci.* **75**, 2478 (1978).
- [20] N. H. Mendelson, J. J. Thwaites, J. O. Kessler, and C. Li, *J. Bacteriol.* **177**, 7060 (1995).

- [21] N. H. Mendelson, B. Salhi, and C. Li, in *Bacteria as Multicellular Organisms*, ed. J. A. Shapiro and M. Dworkin (Oxford University Press, New York, 1997) p. 339
- [22] N. H. Mendelson, *Environ. Microbiology* **1**, 471 (1999).
- [23] N. H. Mendelson, J. E. Sarlls, C. W. Wolgemuth, and R. E. Goldstein, *Phys. Rev. Lett.* **84**, 1627 (2000).
- [24] N. H. Mendelson, J. E. Sarlls, and J. J. Thwaites, *Microbiology* **147**, 929 (2001).
- [25] N. H. Mendelson, D. Morales, and J. J. Thwaites, *BMC Microbiology* **2**, 1 (2002).
- [26] N. H. Mendelson, P. Shipman, D. Roy, L. Chen, and J. J. Thwaites, *BMC Microbiology* **3**, 18 (2003).
- [27] K. Kumada, A. Iwama, and T. Takahashi, *Microbes and Environments* **11**, 1 (1996) [in Japanese].
- [28] S. Takeuchi, W. R. DiLuzio, D. B. Weibel, and G. M. Whitesides, *Nano Lett.* **5**, 1819 (2005).
- [29] B. Peters, A. Heyden, A. T. Bell, and A. Chakraborty, *J. Chem. Phys.* **120**, 7877 (2004).
- [30] C. W. Wolgemuth, R. E. Goldstein, and T. R. Powers, *Physica D* **190**, 266 (2004).
- [31] A. Goriely and S. Neukirch, *Phys. Rev. Lett.* **97**, 184302 (2006).
- [32] D. E. Moulton, T. Lessinnes, and A. Goriely, *J. Mech. Phys. Solids* **61**, 398 (2013).